引用格式：JIANG Jia, GENG Minming, LIU Qiang, et al. Design of a Reconfigurable Optical Filter Based on Triple-ring-assisted Mach-Zenhnder Interferometer with Large Bandwidth Tuning Capability[J]. Acta Photonica Sinica, 2021, 50(7): 0713002
蒋佳,耿敏明,刘嫱,等. 基于三环辅助Mach-Zehnder干涉仪的带宽可调滤波器设计[J].光子学报,2021,50(7):0713002

基于三环辅助Mach-Zehnder干涉仪的带宽可调滤波器设计

蒋佳[1,2],耿敏明[1,2,3,4],刘嫱[1,2,3],张振荣[1,2,3]
(1 广西大学 计算机与电子信息学院,南宁 530004)
(2 广西多媒体通信与网络技术重点实验室,南宁 530004)
(3 广西大学 广西高校多媒体通信与信息处理重点实验室,南宁 530004)
(4 广西信息科学实验中心,广西 桂林 541004)

摘　要:设计了一种基于绝缘体上硅的具有大带宽调谐能力的紧凑型可重构光滤波器。该装置由三个微环辅助马赫-曾德尔干涉仪构成,利用硅的热光效应可以控制微环谐振器的相位,进而同时调节滤波器的带宽和中心波长。用时域有限差分法对器件的性能进行了仿真,仿真结果表明,带宽的调谐范围为1.4～10.6 nm,占自由光谱范围的11.5%～85%;阻带消光比大于20 dB,通带损耗为0.4～0.7 dB,器件尺寸为40 μm×60 μm。

关键词:光滤波器;硅基;马赫-曾德尔干涉仪;微环谐振器;带宽可调
中图分类号:TN256　　**文献标识码**:A　　**doi**:10.3788/gzxb20215007.0713002

Design of a Reconfigurable Optical Filter Based on Triple-ring-assisted Mach-Zenhnder Interferometer with Large Bandwidth Tuning Capability

JIANG Jia[1,2], GENG Minming[1,2,3,4], LIU Qiang[1,2,3], ZHANG Zhenrong[1,2,3]
(1 *School of Computer, Electronics and Information, Guangxi University, Nanning* 530004, *China*)
(2 *Guangxi Key Laboratory of Multimedia Communications and Network Technology, Guangxi University, Nanning* 530004, *China*)
(3 *Key Laboratory of Multimedia Communications and Information Processing of Guangxi Higher Education Institutes, Guangxi University, Nanning* 530004, *China*)
(4 *Guangxi Experiment Center of Information Science, Guilin Guangxi* 541004, *China*)

Abstract: A compact reconfigurable optical filter based on silicon-on-insulator with large bandwidth tuning capability is designed in this paper. The device is based on triple-ring-assisted Mach-Zehnder interferometer. The bandwidth and center wavelength of the device can be tuned at the same time by

Foundation item: National Natural Science Foundation of China (Nos.61965003, 61741504 , 61661004), Guangxi Science Foundation (No. 2018GXNSFAA294133)
First author: JIANG Jia (1994—), male, M. S. degree candicate, mainly focuses on optical communication technology. Email: 2078109394@qq.com
Supervisor (Contact author): GENG Minming (1981—), male, lecture, PhD, mainly focuses on optical communication technology. Email: gengmm@gxu.edu.cn
Received: Dec.28,2020; **Accepted**: Feb.23,2021

reasonably changing the phases of the microring resonators through the thermo-optic effect of silicon. The performance of the proposed device is simulated by finite difference time domain method. The simulation results show that the tuning range of the bandwidth is 1.4 nm to 10.6 nm, which accounts for 11.5% to 85% of the free spectrum range. The stopband extinction ratio is greater than 20 dB, and the passband loss is 0.4 dB to 0.7 dB, the footprint of the device is about 40 μm×60 μm.

Key words: Optical filter; Silicon-on-insulator; Mach-Zehnder interferometer; Microring resonator; Tunable bandwidth

OCIS Codes: 130.7408; 130.3120; 230.7370; 230.7380

0 Introduction

In the past decades, especially in the twenty years of the new century, the silicon photonics has been developing extremely rapidly, due to its superiorities in many aspects, such as fabrication technology, integration density, excellent performance, application diversity and so on[1-4]. Many devices and circuits based on silicon photonics have been proposed and demonstrated[5-6], which can be widely used in optical fiber communications[7], optical interconnect[8], microwave photonics[9], optical sensing[10], optical neural network[11], quantum communication[12], etc. As various applications become more and more intelligent, the reconfigurability is a key performance for the devices and circuits to meet the requirements of different applications[13]. As the most fundamental element, the reconfigurable optical filters based on silicon photonics have been reported with different schemes, e.g., AWG, Bragg-grating, Mach-Zehnder Interferometer (MZI), Microring Resonators (MRR), etc. The schemes based on AWG[14, 15] have advantages in multi-wavelength alignment and translation of all channels. But to some extent, the flexibility of the filters based on AWG is relatively weak when dealing with single channel is required. The schemes based on Bragg-grating[16, 17] can be Free Spectrum Range (FSR) free which is desired in ultra-wideband applications of fiber communications and microwave photonics. But the footprint of the devices based on Bragg-grating is relatively large, which makes the tuning power consumption quite high. The schemes based on MZI, MRR or a mixture of the two structures[18-28] have advantages in flexibility, scalability, footprint and power consumption. To tune both the bandwidth and wavelength, the optical filters based on cascaded high-order microring resonators or ring-assisted MZI have been proposed[20-28]. The bandwidth tunability performance of the proposed filters is limited. In the proposed filters, the maximum Bandwidth Tuning Range (BTR) is about 1.44 nm reported in Ref.[22], which may be not large enough for the applications in the 400 Gbps/1 Tbps flexible optical communication networks[29]. In this paper, a compact silicon reconfigurable optical filter based on triple-ring-assisted MZI with ultra-large bandwidth tuning range is proposed.

1 Selection and optimization of scheme

As mentioned above, there are mainly two kinds of schemes to design the bandwidth-tunable optical filter. One is based on ring-assisted MZI, the other is based on multiple cascaded microring resonators. The performance parameters of the optical filters based on the two schemes are summarized in Table 1. The BTRs of the two schemes are almost the same. But in general, the filters based on ring-assisted MZI have an edge in terms of the proportion of BTR in the whole FSR, which is more suitable for designing optical filter with large BTR. Thus, the scheme based on ring-assisted MZI is selected in this paper.

To meet the requirements of optical fiber communication systems[30], the Stopband Extinction Ratio (SER) should be larger than 20 dB and the passband loss lower than 1 dB during the reconstruction of the wavelength and bandwidth of the optical filter. The number of microring resonator in a ring-assisted MZI is the key to the performance of the optical filters based on it. The optical filters based on double-ring-assisted MZI are reported in Ref.[21-24], but the SER or PL may deteriorate when changing the phase of the microring resonator to tune the bandwidth or wavelength of the filter, which makes the performance of the filter unstable. To enlarge the BTR and make the filter more stable, one more microring resonator is added to the double-ring-assisted MZI to form an asymmetric phase control structure.

Table 1 The summarization of performance of different schemes

Scheme	BW_{max} / FSR	Tunable BW / nm	Ref.
MRRs in an MZI	0.88 nm / 9 nm	0.46～0.88	[21]
MRRs in an MZI	1.44 nm / 1.6 nm	0.16～1.44	[22]
MRRs in an MZI	1.12 nm / 8.5 nm	0.37～1.12	[23]
MRRs in an MZI	0.113 nm / 0.256 nm	0.033～0.113	[24]
Cascaded rings	1 nm / 7.2 nm	0.0928 ～1	[25]
Cascaded rings	1.2 nm / 70.8 nm	0.3～1.2	[26]
Cascaded rings	0.16 nm / 16 nm	0.12～0.16	[27]
Cascaded rings	0.64 nm / 1.8nm	0.056～0.64	[28]

2 Theoretical analysis and optimization of key parameters

The structure of the designed optical filter, which is based on triple-ring-assisted MZI, is shown in Fig.1. The inputs are denoted by X_1 and X_2, and the outputs are denoted by Y_1 and Y_2. X_2 is zero during the process of design and simulation. The power coupling ratios of the 3-dB couplers named K_1 and K_2 are k_1 and k_2, respectively. The three MRRs are the key phase control units in the filter. The MRR called R_A is coupled with the upper arm of the MZI, and R_B as well as R_C is coupled with the lower arm. Thus, the structure of the optical filter is asymmetric, which makes the bandwidth of the filter can be tuned. In order to control the coupling strength and phase conveniently, the race-track structure is selected. The three yellow areas in Fig.1 are used to change the phases of the MRRs, named θ_A, θ_B and θ_C, respectively, to tune the center wavelength of the optical filter by thermo-optic or electro-optic effect of silicon[1]. The electro-optic effect usually induces extra loss caused by the absorption of the free carriers[31] whereas the thermo-optic effect does not induce any extra loss. Thus, the thermo-optic effect is selected in this paper.

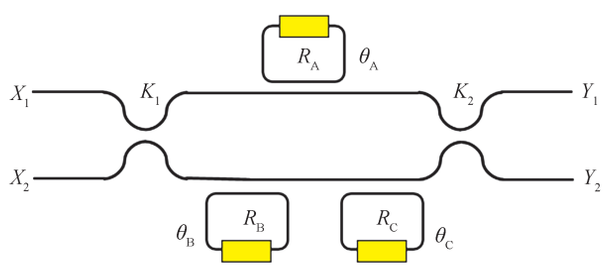

Fig. 1 Schematic of the proposed device based on triple-ring-assisted MZI

According to the transfer-matrix method[31-32], the relationship between the inputs and outputs of the filter meets the following equation.

$$\begin{bmatrix} Y_1 \\ Y_2 \end{bmatrix} = \begin{bmatrix} c_2 & -\mathrm{j}s_2 \\ -\mathrm{j}s_2 & c_2 \end{bmatrix} \begin{bmatrix} H_1(z) & 0 \\ 0 & H_2(z) \end{bmatrix} \begin{bmatrix} c_1 & -\mathrm{j}s_1 \\ -\mathrm{j}s_1 & c_1 \end{bmatrix} \begin{bmatrix} X_1 \\ X_2 \end{bmatrix} = \begin{bmatrix} c_1c_2H_1(z) - s_1s_2H_2(z) & -\mathrm{j}\left(s_1c_2H_1(z) + c_1s_2H_2(z)\right) \\ -\mathrm{j}\left(c_1s_2H_1(z) + s_1c_2H_2(z)\right) & -s_1s_2H_1(z) + c_1c_2H_2(z) \end{bmatrix} \begin{bmatrix} X_1 \\ X_2 \end{bmatrix} \tag{1}$$

In Eq. (1), the parameters of c_l and s_l ($l = 1$ and 2) satisfy the following equations.

$$c_l = \sqrt{1-k_l}, s_l = -\mathrm{j}\sqrt{k_l}, l = 1, 2 \tag{2}$$

To make the performance of the proposed filter better, the power coupling ratios of K_1, as well as K_2, is equal to 1∶1, which means the structures of the two 3-dB couplers are the same and the subscript of k, c and s can be omitted. The system transfer functions of the proposed filter, which are the keys to analyze the performance of the filter, are obtained as follows when X_2 is zero.

$$H_{Y_1}(z) = \left|\frac{Y_1(z)}{X_1(z)}\right| = c^2H_1(z) - s^2H_2(z) \tag{3}$$

$$H_{Y_2}(z)=\left|\frac{Y_2(z)}{X_1(z)}\right|=csH_1(z)+scH_2(z) \tag{4}$$

Here, $H_1(z)$ is the transfer function of the upper arm coupled with R_A, and $H_2(z)$ is the transfer function of the lower arm coupled with R_B and R_C. Both $H_1(z)$ and $H_2(z)$ can be obtained by transfer-matrix method and shown below.

$$H_1(z)=\frac{\rho_A-z^{-1}e^{-j\theta_A}}{1-\rho_A z^{-1}e^{-j\theta_A}} \tag{5}$$

$$H_2(z)=\frac{\rho_B\rho_C-\left(\rho_B e^{-j\theta_C}+\rho_C e^{-j\theta_B}\right)z^{-1}+e^{-j\left(\theta_B+\theta_C\right)}z^{-2}}{1-\left(\rho_B e^{-j\theta_B}+\rho_C e^{-j\theta_C}\right)z^{-1}+\rho_B\rho_C e^{-j\left(\theta_B+\theta_C\right)}z^{-2}} \tag{6}$$

Here, the power coupling ratios and transmission coefficients between the resonators and straight waveguides are denoted by k_i and ρ_i (i=A, B and C), respectively. The relationship between k_i and ρ_i is shown below.

$$\rho_i=\sqrt{1-k_i},\ i=\mathrm{A,B}\ and\ \mathrm{C} \tag{7}$$

In order to get the system transfer functions, take Eqs. (5) and (6) into Eqs. (3) and (4). To simplify the results, let $\rho_B=\rho_C$, and $\theta_B=-\theta_C$, and the system transfer functions are obtained as follows.

$$H_{Y_1}(z)=\frac{0.5(M_1-M_2z^{-1}+M_3z^{-2}+M_1e^{-j\theta_A}z^{-3})}{1-(2\rho_B\cos\theta_B+\rho_A e^{-j\theta_A})z^{-1}+(\rho_B^2+2\rho_A\rho_B\cos\theta_B e^{-j\theta_A})z^{-2}-\rho_B^2\rho_A e^{-j\theta_A}z^{-3}} \tag{8}$$

Here, $M_1=\rho_A-\rho_B^2$, $M_2=2\rho_A\rho_B\cos\theta_B+e^{-j\theta_A}-2\rho_B\cos\theta_B-\rho_A\rho_B^2e^{-j\theta_A}$ and $M_3=2\rho_B\cos\theta_B e^{-j\theta_A}+\rho_A\rho_B^2-2\rho_A\rho_B\cos\theta_B e^{-j\theta_A}-1$.

$$H_{Y_2}(z)=\frac{0.5(N_1-N_2z^{-1}+N_3z^{-2}-N_1e^{-j\theta_A}z^{-3})}{1-(2\rho_B\cos\theta_B+\rho_A e^{-j\theta_A})z^{-1}+(\rho_B^2+2\rho_A\rho_B\cos\theta_B e^{-j\theta_A})z^{-2}-\rho_B^2\rho_A e^{-j\theta_A}z^{-3}} \tag{9}$$

Here, $N_1=\rho_A+\rho_B^2$, $N_2=2\rho_B\cos\theta_B+\rho_B^2\rho_A e^{-j\theta_A}+2\rho_A\rho_B\cos\theta_B+e^{-j\theta_A}$ and $N_3=2\rho_B\cos\theta_B e^{-j\theta_A}+\rho_A\rho_B^2+2\rho_A\rho_B\cos\theta_B e^{-j\theta_A}+1$.

Using the system transfer functions, the response of the proposed optical filter can be calculated and optimized. The bandwidth can be tuned continuously by tuning θ_B and θ_C while keeping θ_A equal to 0, θ_B equal to $-\theta_C$ and ρ_i constant. According to the system transfer functions, ρ_i and θ_i are the key parameters affecting the performance of the filter. Here, the impact of ρ_i is analyzed first and the results are shown in Figs.2 (a)~(e), respectively. First, the relationship between ρ_A, ρ_B and the Stopband Extinction Ratios (SER) of two outputs are analyzed and depicted in Figs.2 (a) and (b). In both pictures, there are some blank areas, in which the response curve of the filter will be distorted and the corresponding parameters cannot be used to design the filter. The SER may fluctuate during the process of bandwidth adjustment. The minimum value of the SER, denoted by SER_{min}, should be larger than 20 dB to meets the requirement of optical fiber communication systems[30]. The effective regions meeting the condition mentioned above are the lower right region of Fig. 2 (a) and the lower left region of Fig.2 (b), which are marked with a single white dotted line in both pictures. The coordinates of the intersections between the coordinate axis or boundary and the white dotted line are indicated. The overlapping part of the effective regions of Figs. 2 (a) and (b), marked with A, is exactly the effective region

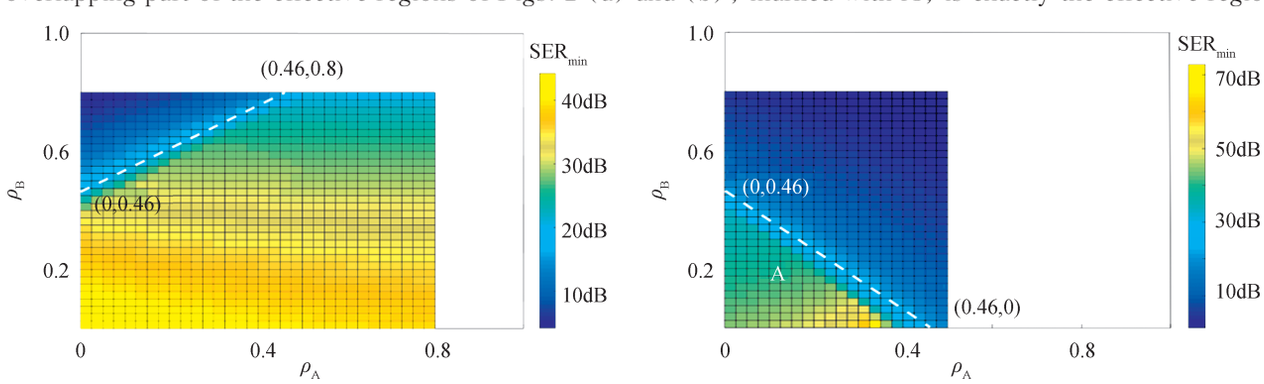

(a) The minimum SER of Y_1 (b) The minimum SER of Y_2

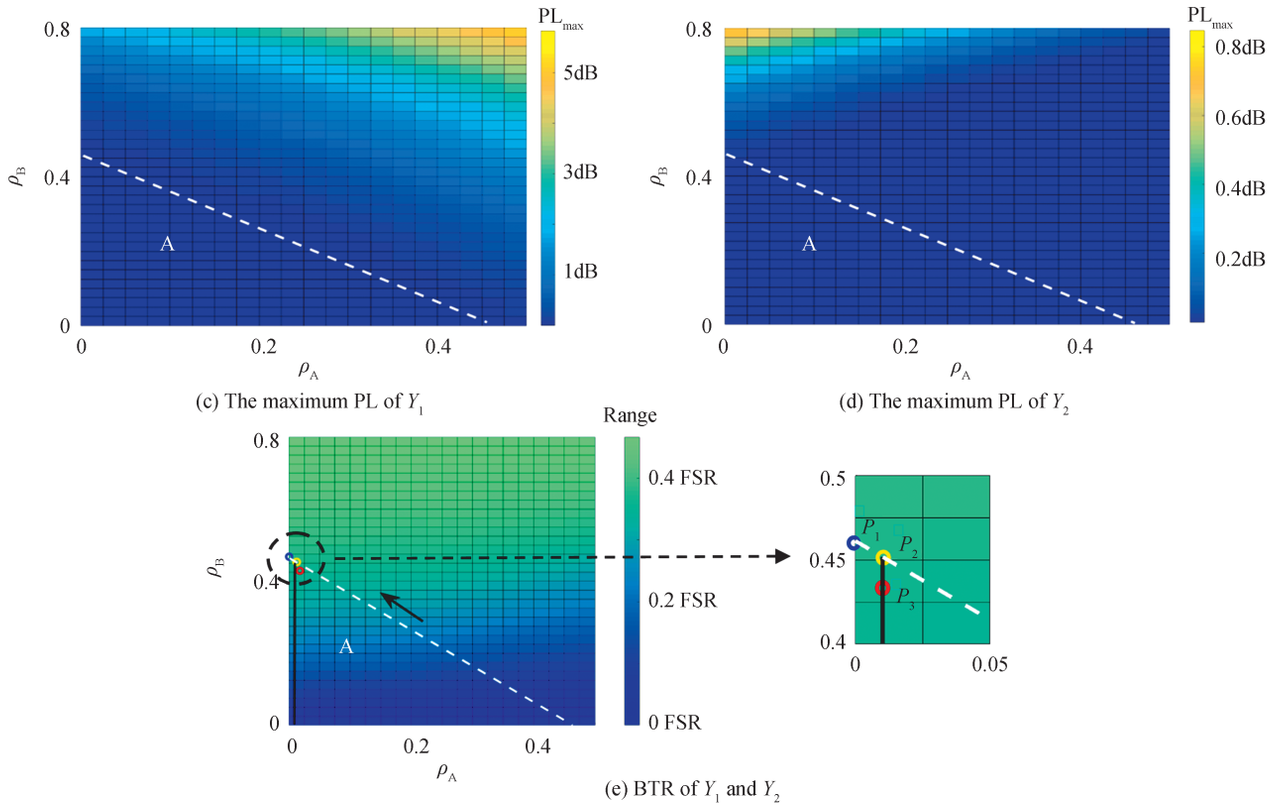

Fig.2 The influence of ρ_A and ρ_B on the performance of the optical filter

in Fig.2 (b), which is the key to the subsequent analysis and design.

The relationship between ρ_A, ρ_B and the maximum loss of passband of the two outputs named PL_{max} is analyzed and shown in Figs.2 (c) and (d). It can be seen that the PL_{max} in the region A is smaller than 1 dB in both pictures, which meets the performance requirement.

The relationship between ρ_A, ρ_B and BTR is shown in Fig. 2 (e). The BTR is normalized by the proportion of the whole FSR. The BTRs of the two outputs are the same and will get larger in the direction of the black arrow and reach the maximum value in the region A.

According to the analysis above, in order to ensure the performance of SER and maximize the BTR, the ideal parameter combination of (ρ_A, ρ_B) is (0, 0.46), labeled with P_1 in Fig. 2 (e).

The phases of the microring resonators can be used to tune the central wavelength of the filter. Here, the output of Y_2 is selected to make a detailed explanation. The system transfer function of Y_2 is rewritten as follows and an extra phase θ is applied to the three resonators simultaneously.

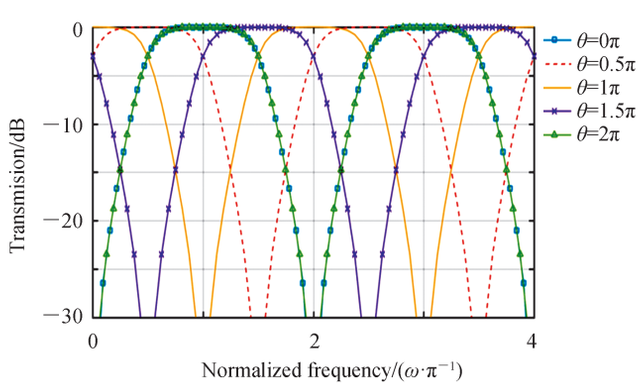

Fig.3 Normalized central frequency is shifted with the change of the extra phase θ applied on the three resonators

$$H_{Y_2}(z)=\frac{0.5\left(N_1-N_2z^{-1}\mathrm{e}^{-\mathrm{j}\theta}+N_3z^{-2}\mathrm{e}^{-\mathrm{j}2\theta}-N_1\mathrm{e}^{-\mathrm{j}\theta_A}z^{-3}\mathrm{e}^{-\mathrm{j}3\theta}\right)}{1-(2\rho_B\cos\theta_B+\rho_A\mathrm{e}^{-\mathrm{j}\theta_A})z^{-1}\mathrm{e}^{-\mathrm{j}\theta}+(\rho_B^2+2\rho_A\rho_B\cos\theta_B\mathrm{e}^{-\mathrm{j}\theta_A})z^{-2}\mathrm{e}^{-\mathrm{j}2\theta}-\rho_B^2\rho_A\mathrm{e}^{-\mathrm{j}\theta_A}z^{-3}\mathrm{e}^{-\mathrm{j}3\theta}} \quad (10)$$

The response of Eq. (10) is plotted in Fig. 3, and the results show that the normalized central frequency of the filter will shift $\theta/2\pi$. When $\theta = 2\pi$, the shifting range of the central frequency will be the whole FSR, which makes the two curves ($\theta = 0$ and $\theta = 2\pi$) coincide. The situation of Y_1 is the same as that of Y_2.

3 Simulation and optimization

3.1 Structure design and optimization

According to the analysis above, the structure of the proposed optical filter is designed and optimized using Finite Difference Time Domain (FDTD) method. The channel-type waveguide with height of 250 nm is chosen. The race-track resonator named R_i shown in Fig. 4 is consisted of four arcs with radius of r_i, two vertical straight waveguides with length of L_{mi} and two horizontal straight waveguides with length of L_{ni} (i=A, B and C).

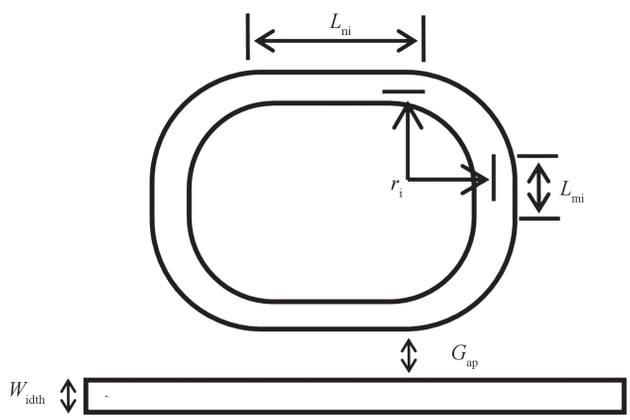

Fig.4 The structure of the race-track microring resonator

As the discussion on the Fig. 2 (e), the smaller the ρ_A, the larger the BTR. In Fig. 4, W_{idth}, G_{ap} and L_{nA} are the key structural parameters that affect ρ_A. To find out the minimum value of ρ_A named ρ_{Amin}, FDTD method is used to calculate the value of ρ_{Amin} in different combinations of these structural parameters and the results are shown in Fig. 5. The optimum combination of the three structural parameters is labeled with black circle in the picture, which means ρ_{Amin} will be 0.008 when W_{idth} is 0.4 μm, G_{ap} is 130 nm and L_{nA} is 5.85 μm. A black line where ρ_A equals 0.008 is drawn in Fig. 2 (e) and it intersects with the white dotted line at P_2 (0.008, 0.45). Here, P_2 can meet the requirements of SER and PL, and make the BTR largest. But there is about 5% error in the fabrication of waveguide. This factor is taken into account in the simulation, and P_3 (0.008, 0.43) is selected. Thus, the value of ρ_B as well as ρ_C is 0.43, and L_{nB} and L_{nC} are calculated to be 3.69 μm, while keeping W_{idth} equal to 0.4 μm and G_{ap} equal to 130 nm.

The transmission coefficient ρ_r will change with the wavelength, which will influence the performance of

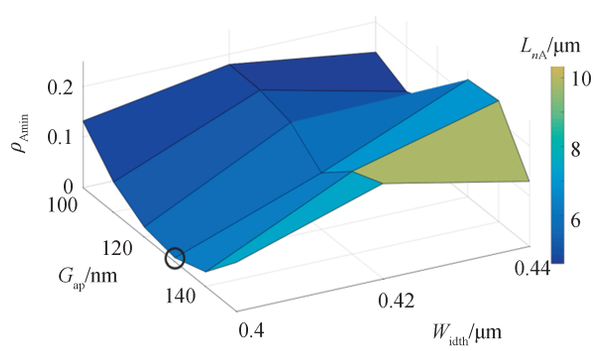

Fig.5 The value of ρ_{Amin} with different W_{idth}, G_{ap} and L_{nA}

the filter. The dispersion effect is introduced into the Eqs. (8) and (9). The relationship between FSR and SER is discussed to take into account the influence mentioned above and the results are shown in Fig. 6. The larger the FSR, the smaller the minimum SER. To make sure the performance of the filter stable, the value of FSR is selected to be 12.5 nm. Using the resonance condition, L_{mA} is calculated to be 0.37 μm, L_{mB} as well as L_{mC} to be 2.75 μm and r_i to be about 5 μm (i=A, B and C).

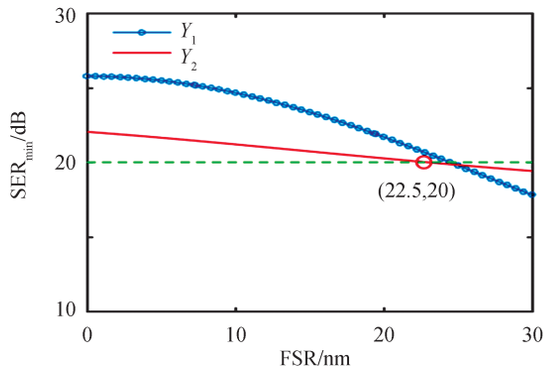

Fig. 6 The relationship between the FSR and the minimum SER of the two outputs

During the analysis in Section 2, the phase θ_C or θ_B is negative ($\theta_C = -\theta_B$), which is difficult to realize. To overcome this difficulty, the initial phase values of the three resonators should be π but not 0. The initial phase π can be realized by changing the refractive index of the resonators through the thermo-optic effect. Around 1 550 nm, and when the temperature is between 300 K to 550 K, the empirical formula of the relationship between the thermo-optic coefficient and temperature of silicon is shown below [33].

$$\frac{dn}{dT} = 9.48 \times 10^{-5} + 3.47 \times 10^{-7} \times T - 1.49 \times 10^{-10} \times T^2 \quad (K^{-1}) \tag{11}$$

The relationship between the initial phase and the change of the refractive index Δn is simulated and shown in Fig. 7. It means that the initial phase can be π when Δn is 0.008, and the temperature change of the waveguide is about 40 K according to the Eq. (11). When tuning the bandwidth of the filter, R_B can be heated and R_C can be cooled, or vice versa, to keep θ_C equal to $2\pi - \theta_B$, which is the same as θ_C equal to $-\theta_B$ from the perspective of phase.

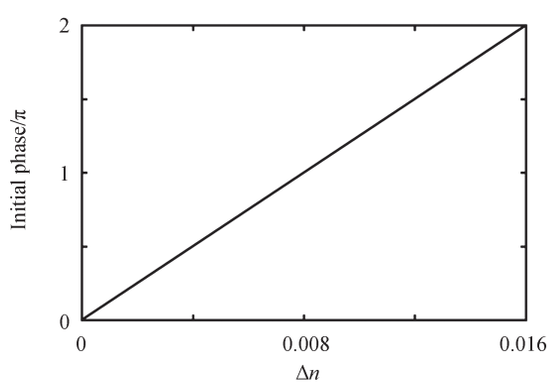

Fig.7 The relationship between the initial phase and Δn

To lower the power consumption of the device, the initial phase of R_A can be realized by inserting a phase shifter into the straight waveguide of R_A. The phase shifter is composed by two linear tapers as plotted in Fig. 8. The values of W_s and L_s are determined by FDTD method, which are 0.54 μm and 5 μm, respectively.

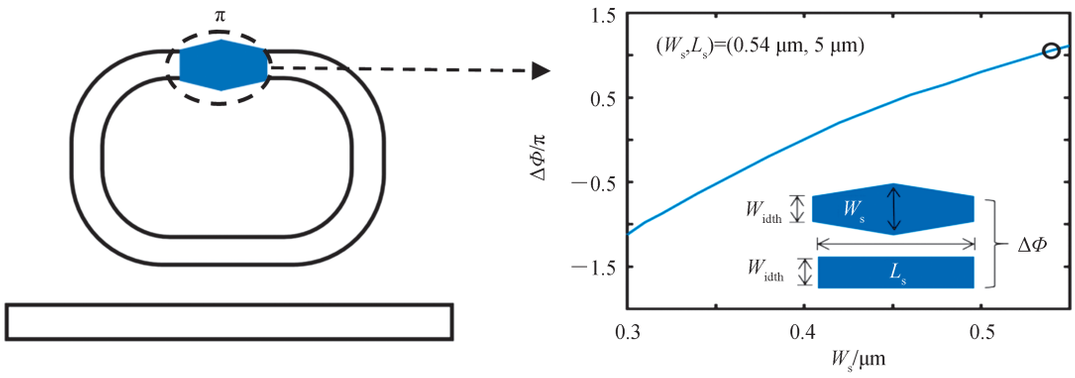

Fig.8 The structure of the phase shifter

3.2 Simulation of the optical filter with large bandwidth tuning capability

The structure parameters of the proposed filter are listed in Table 2 and its footprint is about 40 μm×60 μm. The performance of the device is simulated by FDTD method and only TE mode is considered. The results are shown in Fig. 9. The bandwidth of the two ports is continuously changed with θ_B and θ_C. The SER is better than 20 dB and the PL is 0.4 dB to 0.7 dB.

Table 2 The simulation settings of the filter

Item	Value
Waveguide type	Channel
Waveguide height	0.25 μm
r_A, r_B and r_C	5 μm
W_{idth}	0.4 μm
G_{ap}	130 nm
Refractive index of silicon	3.507
Refractive index of silica	1.447
Polarization	TE
L_{nA} / L_{nB} and L_{nC}	5.85 μm/3.69 μm
L_{mA} / L_{mB} and L_{mC}	0.37 μm/2.75 μm

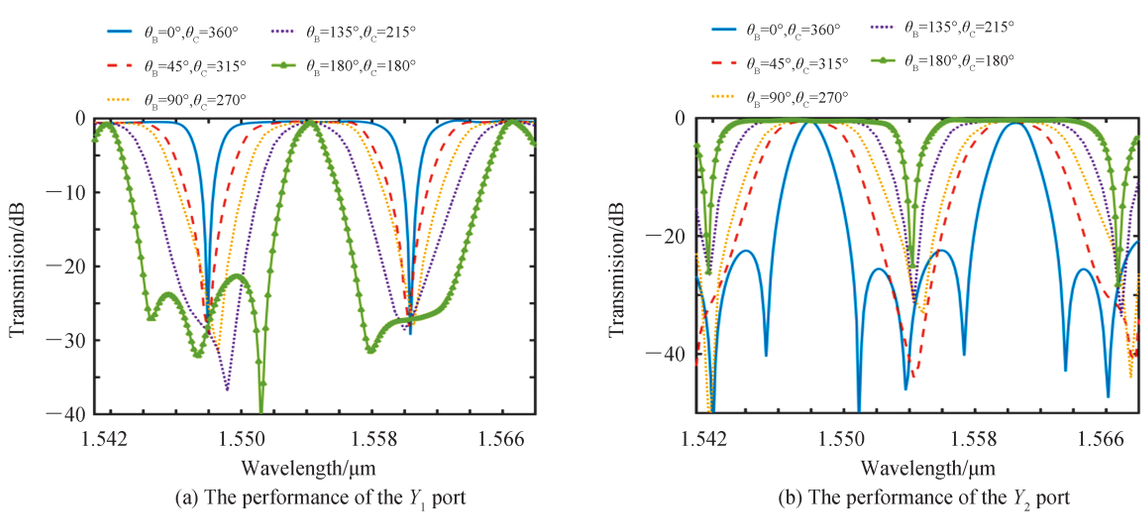

Fig. 9 The performance of the optical filter with different θ_B and θ_C

Both the bandwidth and wavelength can be reconstructed at the same time by tuning the phase of the resonators. The bandwidth is controlled by θ_B and θ_C, and the wavelength is controlled by an extra phase θ applied to the three resonators simultaneously. The results simulated by FDTD method are shown in Fig. 10.

The extra phase θ is changed between 0 to 2π with step of π, and θ_B changed between 0 to π with step of $\pi/2$ while keeping θ_C equal to $2\pi - \theta_B$. It can be seen that the wavelength shifted about 12.5 nm to the right, meanwhile, the bandwidth is changed from 1.4 nm to 10.6 nm. Thus, the maximum phase shift of the resonators is 3π, which corresponds to the change of waveguide temperature about 120°.

Both the bandwidth and wavelength can be reconstructed at the same time by tuning the phase of the resonators. The bandwidth is controlled by θ_B and θ_C, and the wavelength is controlled by an extra phase θ applied to the three resonators simultaneously. The results simulated by FDTD method are shown in Fig. 10. The extra phase θ is changed between 0 to 2π with step of π, and θ_B changed between 0 to π with step of $\pi/2$ while keeping θ_C equal to $2\pi - \theta_B$. It can be seen that the wavelength shifted about 12.5 nm to the right, meanwhile, the bandwidth is changed from 1.4 nm to 10.6 nm. Thus, the maximum phase shift of the resonators is 3π, which corresponds to the change of waveguide temperature about 120°.

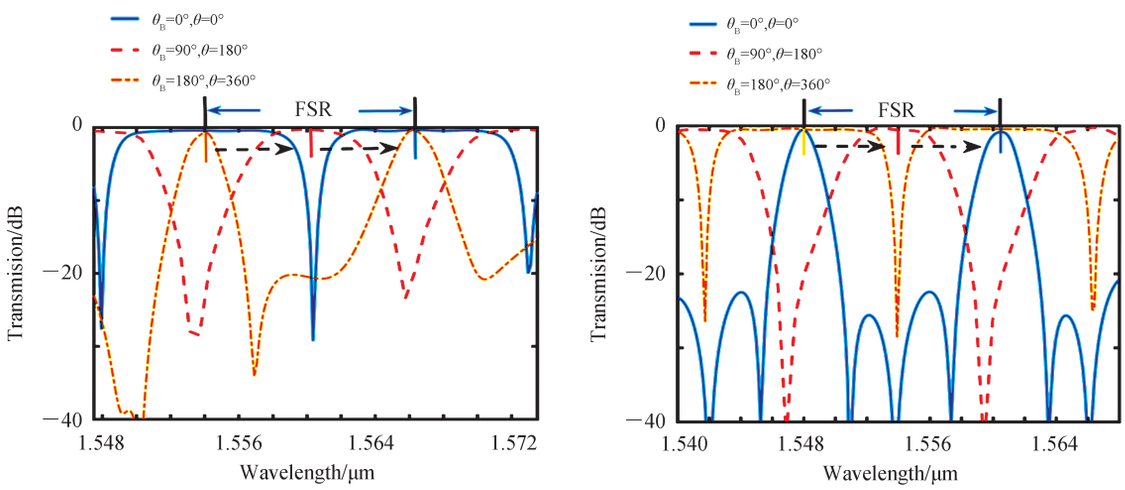

(a) The performance of the Y_1 port (b) The performance of the Y_2 port

Fig.10 The reconfigurations of the wavelength and the bandwidth of the filter

4 Conclusion

In this paper, a reconfigurable optical filter based on triple-ring-assisted MZI with large bandwidth tuning capacity is designed. The system transfer function of the filter is derived using transfer-matrix method. The performance and the structure of the device are analyzed and optimized using the FDTD method. The SER is better than 20 dB, and the PL is less than 0.7 dB. The footprint of the device is about 40 μm×60 μm. By changing the refractive index of the resonators through thermo-optic effect, the center wavelength and the bandwidth can be reconstructed at the same time. The bandwidth of the filter can be tuned between 1.4 nm to 10.6 nm, which accounts for 11.5% to 85% of the FSR.

References

[1] SOREF R. The past, present, and future of silicon photonics[J]. IEEE Journal of selected topics in quantum electronics, 2006, 12(6): 1678-1687.

[2] ABSIL P P, VERHEYEN P, DE HEYN P, et al. Silicon photonics integrated circuits: a manufacturing platform for high density, low power optical I/O's[J]. Optics Express, 2015, 23(7): 9369-9378.

[3] LU Z, JHOJA J, KLEIN J, et al. Performance prediction for silicon photonics integrated circuits with layout-dependent correlated manufacturing variability[J]. Optics Express, 2017, 25(9): 9712-9733.

[4] ZHANG Y, SAMANTA A, SHANG K, et al. Scalable 3D silicon photonic electronic integrated circuits and their applications[J]. IEEE Journal of Selected Topics in Quantum Electronics, 2020, 26(2): 1-10.

[5] DONG P, CHEN Y K, DUAN G H, et al. Silicon photonic devices and integrated circuits[J]. Nanophotonics, 2014, 3(4-5): 215-228.

[6] HELKEY R, SALEH A A M, BUCKWALTER J, et al. High-performance photonic integrated circuits on silicon[J]. IEEE Journal of Selected Topics in Quantum Electronics, 2019, 25(5): 1-15.

[7] LI Jianhui, ZHANG Yongtang, WANG Fang. The design of a high quality and minimum wavelength of ultra-low-loss

tapered optical fiber[J]. Acta Photonica Sinica, 2016, 45(7): 0706005.

[8] JIA H, ZHOU T, FU X, et al. Four-port mode-selective silicon optical router for on-chip optical interconnect[J]. Optics Express, 2018, 26(8): 9740-9748.

[9] WANG Dong, DAI Bo, REN Liqing, et al . A modulation sheme to generate 24-GHz-Band millimeter-wave-band ultra-wideband signal by using Mach Zehnder modulator[J]. Acta Photonica Sinica, 2015, 44(9): 0906001.

[10] LI Jiawen, ZHANG Jiahong, XU Xiaoping, et al. Integrated optical waveguide Mach-Zehnder interferometer power frequency intensive electric field sensor[J]. Acta Photonica Sinica, 2019, 48(9): 0913001.

[11] JHA A, HUANG C, PRUCNAL P R. Reconfigurable all-optical nonlinear activation functions for neuromorphic photonics[J]. Optics Letters, 2020, 45(17): 4819-4822.

[12] WEI K, LI W, TAN H, et al. High-speed measurement-device-independent quantum key distribution with integrated silicon photonics[J]. Physical Review X, 2020, 10(3): 031030.

[13] XIE Y, SHI Y, LIU L, et al. Thermally-reconfigurable silicon photonic devices and circuits[J]. IEEE Journal of Selected Topics in Quantum Electronics, 2020, 26(5): 1-20.

[14] TONDINI S, CASTELLAN C, MANCINELLI M, et al. Methods for low crosstalk and wavelength tunability in arrayed-waveguide grating for on-silicon optical network[J]. Journal of Lightwave Technology, 2017, 35(23): 5134-5141.

[15] LIU Y, LI Z, LI D, et al. Thermo-optic tunable silicon arrayed waveguide grating at 2-μm wavelength band[J]. IEEE Photonics Journal, 2020, 12(4): 1-8.

[16] ST-YVES J, BAHRAMI H, JEAN P, et al. Widely bandwidth-tunable silicon filter with an unlimited free-spectral range [J]. Optics Letters, 2015, 40(23): 5471-5474.

[17] IKEDA K, KONOIKE R, SUZUKI K, et al. 2×2 16-ch silicon photonics wavelength-selective switch based on waveguide gratings[J]. Optics Express, 2020, 28(18): 26861-26869.

[18] YANG L, XIA Y, ZHANG F, et al. Reconfigurable nonblocking 4-port silicon thermo-optic optical router based on Mach-Zehnder optical switches[J]. Optics Letters, 2015, 40(7): 1402-1405.

[19] WANG H, DAI J, JIA H, et al. Polarization-independent tunable optical filter with variable bandwidth based on silicon-on-insulator waveguides[J]. Nanophotonics, 2018, 7(8): 1469-1477.

[20] SHOMAN H, JAYATILLEKA H, PARK A H K, et al. Compact wavelength-and bandwidth-tunable microring modulator[J]. Optics Express, 2019, 27(19): 26661-26675.

[21] DING Y, PU M, LIU L, et al. Bandwidth and wavelength-tunable optical bandpass filter based on silicon microring-MZI structure[J]. Optics Express, 2011, 19(7): 6462-6470.

[22] ORLANDI P, FERRARI C, STRAIN M J, et al. Reconfigurable silicon filter with continuous bandwidth tunability[J]. Optics Letters, 2012, 37(17): 3669-3671.

[23] SHEN L, GUO Z, LU L, et al. Reconfigurable silicon optical filters using a dual-ring assisted Mach-Zehnder interferometer based 16×16 switch[C].2017 Asia Communications and Photonics Conference (ACP), IEEE, 2017: 1-3.

[24] LI J, YANG S, CHEN H, et al. Reconfigurable rectangular filter with continuously tunable bandwidth and wavelength [J]. IEEE Photonics Journal, 2020, 12(4): 1-9.

[25] ONG J R, KUMAR R, MOOKHERJEA S. Ultra-high-contrast and tunable-bandwidth filter using cascaded high-order silicon microring filters[J]. IEEE Photonics Technology Letters, 2013, 25(16): 1543-1546.

[26] DAI T, WANG G, JIANG J, et al. Bandwidth tunable filter with large bandwidth and wavelength tuning range[C].2018 Optical Fiber Communications Conference and Exposition (OFC), IEEE, 2018: 1-3.

[27] SHEN H, KHAN M H, FAN L, et al. Eight-channel reconfigurable microring filters with tunable frequency, extinction ratio and bandwidth[J]. Optics Express, 2010, 18(17): 18067-18076.

[28] POULOPOULOS G, GIANNOULIS G, ILIADIS N, et al. Fully flexible filtering element on SOI with 7~80 GHz bandwidth tunability and full FSR tuning[C].2018 Optical Fiber Communications Conference and Exposition (OFC), IEEE, 2018: 1-3.

[29] PINCEMIN E, SONG M, LOUSSOUARN Y, et al. Towards 400G/1T flexible optical transport networks[C].2013 15th International Conference on Transparent Optical Networks (ICTON), IEEE, 2013: 1-13.

[30] SIMMONS J M. Optical network design and planning[M]. Springer, 2014.

[31] SOREF R, BENNETT B. Electrooptical effects in silicon[J]. IEEE Journal of Quantum Electronics, 1987, 23(1): 123-129.

[32] MADSEN C K, ZHAO J H. Optical filter design and analysis[M]. New York: Wiley, 1999.

[33] COCORULLO G, DELLA CORTE F G, RENDINA I. Temperature dependence of the thermo-optic coefficient in crystalline silicon between room temperature and 550 K at the wavelength of 1523 nm[J]. Applied Physics Letters, 1999, 74(22): 3338-3340.